Springer
KSME

Journal of Mechanical Science and Technology 30 (1) (2016) 381~396
www.springerlink.com/content/1738-494x(Print)/1976-3824(Online)
DOI 10.1007/s12206-015-1243-2

Design and implementation of a robust FNN-based adaptive sliding-mode controller for pneumatic actuator systems †

Lian-Wang Lee[1] and I-Hsum Li[2,*]

[1]Department of Mechanical Engineering, Lunghwa University of Science and Technology, Taoyuan, Taiwan, Republic of China
[2]Department of Information Technology, Lee-Ming Institute of Technology, Taipei, Taiwan, Republic of China

(Manuscript Received March 13, 2014; Revised June 6, 2015; Accepted September 13, 2015)

Abstract

An adaptive Fourier neural network sliding mode controller with H_∞ tracking performance (AFNN-SMC+ H_∞) is applied for a Pneumatic actuator system (PAS) to overcome time-varying nonlinear dynamics and external disturbances. Benefiting from the use of orthogonal Fourier basis function, the proposed AFNN has fast estimated convergence speed; also, because AFNN has unique solution, it can avoid falling into the local minimum. The architecture of AFNN can also easily be determined by its clear physical meaning of the neurons. To attenuate the vibration of proportional directional control valve and the adaptive approximation error, the H_∞ tracking design technique is incorporated into the proposed AFNN-SMC. Finally, practical experiments are successfully implemented in position regulation, trajectory tracking, and velocity control of the PAS, which illustrates the effectiveness of the proposed controller.

Keywords: Adaptive control; Fourier neural network; H_∞ tracking performance; Pneumatic actuator system; Sliding mode control

1. Introduction

Over the past few years in industrial motion control applications, a Pneumatic actuator system (PAS) has become popular because of high speed, low energy consumption, and easy maintenance. In addition, due to their low-cost and high ratio of power to weight, a PAS is well-known for linear movement control and robotic manipulator control. Also, a PAS is clean, safe in operation, and no overheating problems. However, the PAS is limited in the difficulty of making stable and accurate motion control. The use of a PAS is traditionally called "end-stop" motion, which is controlled by on/off valves. In the 1950s, researchers started attempting the continuous position control of a PAS. It is unfortunate that limited on low-performance microprocessors and pneumatic components servo-controlled, a PAS was seldom utilized in industry in the last 10 years. In recent years, however, low-cost and high-performance microprocessors and pneumatic components have been accessible, and more complicated control methods in pneumatic system control were possible to be realized [1].

Tracking control of nonlinear systems with uncertain parameters or unknown dynamics has attracted great attention for the last few decades. Adaptive control (AC) was proposed as a way of automatically adjusting the controller parameters in case of the unknown time-varying parameters of a plant. Many adaptive approaches can also be found to take care of uncertainties in the fluid power servo system, which could be classified into two different domains, pneumatic servo system and hydraulic servo system [2-4]. However, the fluid power servo system usually contains much parameter uncertainty caused by the change of environmental temperature and working state. Hence, many researches have applied the AC to the fluid power servo system to cope with these uncertainties. Developing AC is required for a clear mathematical model of the controlled plant, but its robustness is limited by the persistent excitation, the slow time variation, and the strict positiveness. Therefore, researchers have developed ACs with few design limitations, simplified algorithms, which can save computational time, and better robustness. For example, a robust integral of the sign of the error controller and an adaptive controller are synthesized via backstepping method for motion control of a hydraulic rotary actuator [5]. Under the assumption of which the disturbances are periodic-like, Yao et al. presented an adaptive repetitive control based on projection algorithm [6]. Based on a nonlinear system model, a discontinuous projection-based nonlinear adaptive robust backstepping controller was developed to take into account the particular nonlinearities and then a stable parameter adaptation was derived to eliminate the effect of unknown but constant parametric uncertainties [7].

Even though the PAS is simple and inexpensive now, it still

*Corresponding author. Tel.: +886 2 29097811, Fax.: +886 2 29095888
E-mail address: ihsumlee@gmail.com
† Recommended by Associate Editor Jae Cheon Lee

cannot meet the demand of being accurate, versatile, and flexible due to the inborn nonlinearities associated with compressibility of air and complex friction distributions along the cylinders. In addition, unknown time-varying parameters or disturbances have been known to be a challenge of control design. These inborn problems make the PAS hard to acquire high precision motion control. As a result, for the purpose of serving on more complicated motion-control tasks, many researchers [8-11] have explored the PAS for servo system control. Over the last ten years, the input-output feedback linearization technique has been adopted to the PAS [12]. The main idea is first to transform the PAS into a linear system by a nonlinear feedback, and second to use well-known and powerful linear design techniques to fulfill the control design. These techniques, however, can only be applicable to nonlinear systems when the system parameters are precisely known and are unlikely in a practical application. Nearly all kinds of robust control schemes [13] have been proposed to solve the control problems of the PAS, one of which is Sliding mode control (SMC) [14]. The SMC is robust against external disturbances and can provide a systematic approach to maintain stability in the face of modeling imprecision and uncertainty. Nonetheless, the design of traditional SMC has to be required for precise system model, so-called as a model-based control design; therefore, the system dynamic model and the value of uncertain bound for controller design are needed. In general, the SMC suffers from large control chattering that may excite unmodeled high frequency response of the systems so that it has a trade-off between chattering and robustness. Hence, various controllers incorporating SMC have been proposed [15-19] to reduce the chattering. Unfortunately, most of the existing methods require that nonlinear functions of the dynamical system are known, which is impractical in real applications. Furthermore, although SMC rejects uncertainties and disturbances, it suffers from an assumption of which the matching uncertainties or disturbances have to be bounded on norm and the bound should be available for design. Some parameters related the PAS, i.e., the tube length, the cylinder bore diameter, and the critical pressure ratio of chokes flow, are easily measured or obtained from the manufacturer or even can be calculated by extensively received formulas; however, the inner dynamics of the valve flow is still difficult to comprehend with the PAS. Besides, the friction [20, 21] and internal energy change [22], which are necessary in experiments, are quite hard to model and are not yet completely understood. Therefore, due to the complex structure of uncertainties, uncertainty bounds may not be easily obtained, and the traditional SMC cannot be implemented for the PAS.

Lately, many theoretical and practical works have been done in the field of approximate-based control [23-29]. The functional approximation technique is applied to release this model-based requirement. Particularly, Approximate-based adaptive control (ABAC) has been verified and deemed useful to solve control problems of the PAS with time-varying function or unknown nonlinear parameters [30]. In ABAC, the unknown time-varying functions are usually modeled online by several commonly used function approximates, such as multi-layer Neural network (NN) [31], fuzzy neural network [32, 33], wavelet neural network [34], and radial basis function neural network [35, 36]. The NN-based control method has been successfully employed in many applications, but there still are some difficulties in selecting parameters of the activation function and determining network structures. Moreover, the approximation error is affected by the number of layers and neurons so that it is hard to decide specified approximation accuracy. If there are not enough layers and neurons in the network, assuring that the parameters converge to their optimal values may be a problem. On the other hand, having too many layers and neurons causes massive computational burden and inevitably degrades convergent speed. As a result, it deters the on-line control applications and practical implementation feasibility. Thus, for the NNs both the network topology and stability analysis are not easy to carry out [37]. These drawbacks prevent the NNs from being widely used in control design.

To solve the above-mentioned problems and avoid drawbacks of the traditional SMC and NNs, we propose the AFNN-SMC+H_∞ for the motion control design of the PAS with unknown and uncertain bounded parameters. In our proposed control strategy, the technique of input-output feedback linearization is first used to transform the PAS nonlinear model into a linear one. Subsequently, the powerful and universal AFNN approximator is used to approximate the uncertain nonlinear functions of the dynamical system, and the SMC is then applied to stabilize the whole system and attenuate the bounded disturbance. However, the SMC has an inherent limitation of which the matching uncertainties or disturbances have to be bounded for controller design. To release this limitation, the H_∞ tracking design technique [32, 38] based on the relaxed assumption was incorporated into the SMC. Taking advantages of the orthogonal activation basis functions and the clear definition of Fourier series, AFNN has a clear physical meaning and easily determined structure, so that it is over conventional NNs; in addition, AFNN has been proven that there are no local minima for optimization problem [39-41]. Because of the orthogonality of the basis functions, the FNN provides fast convergent speed and it is therefore suitable for real-time implementation [39, 40]. To further decrease the effect caused by approximation error, time-varying dynamics, and external disturbance, an adaptation technique and a compensator with H_∞ tracking performance [32, 38] are included into the AFNN-SMC, named as the AFNN-SMC+H_∞. The weighting update algorithms of the AFNN-SMC+H_∞ are derived from the Lyapunov stabilizing theory. Compared with traditional SMC approaches, which generally require prior knowledge on the upper bound of the uncertainties, the proposed approach not only assures closed-loop stability, but also guarantees the desired H_∞ tracking performance for the overall system based on a much relaxed assumption. Moreover, control chattering happening in the

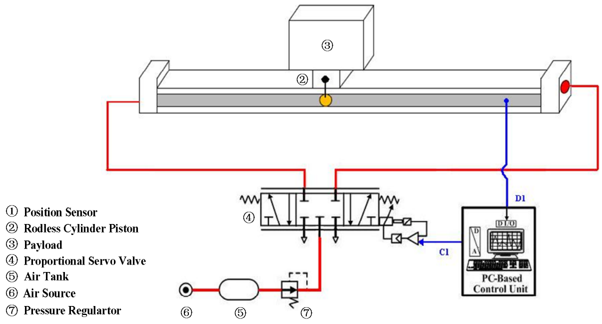

Fig. 1. Pneumatic actuator system schema.

traditional SMC can be greatly lowered by using the proposed approach. The experimental results show that the proposed controller has effective tracking performance despite uncertainties and time-varying payload.

The main contributions of this study are as follows: (1) Thanks to orthogonality of the basis functions, the FNN is not only easy to realize, but also highly improves the convergence speed and the local minimum avoidance. (2) The FNN has a clear physical meaning; therefore, the network topology and the parameter selection of the basis functions become convenient for real applications. (3) The constraint in demanding prior knowledge on upper bounds of the lumped uncertainties is removed. (4) The proposed AFNN-SMC+ H_∞ significantly reduces the control chattering.

2. System description and modeling

2.1 System hardware

A schematic diagram of the PAS is shown in Fig. 1. Table 1 specifies the main components and the system hardware comprises a rodless pneumatic cylinder, a proportional directional control valve, a granite air cushion, and a PC-based control unit. The critical frequency with maximum spool stroke (Festo model MPYE-5-1/8-HF-010B) is 100 Hz and the rodless cylinder in our test rig (Festo model DGPL-25-700-PPV-A-HD40-GK-D2) is with 25 mm bore and 700 mm stroke. The source pressure is regulated at 6×10^5 Pa, and the source temperature is 293 K coming from a dehumidified and filtered process. The rodless cylinder has a built-in linear slider. An optical encoder with a resolution of 20 nm is installed to measure the piston's position, and the default payload is set at 6 kg. The scale's measured signals are feedback to the controlling PC via a decoder IC, Agilent HCTL-2032, and a digital I/O converter. The PC-based control system is implemented on a Pentium III CPU with an ADVANTECH's PCL-726 IO-card which contains D/A converters and digital I/O converter. The proposed control strategy is implemented in an interrupted service routine with 1ms sampling time under MS-DOS environment. The input voltage for the proportion servo valve comes from the controlling PC via D/A converters, and the control law is calculated by a 32-bit Open Watcom C Language program.

Table 1. Main components' specifications of the test rig.

Components	Specifications
Pneumatic cylinder	Diameter: 25 mm Stroke: 600 mm
Proportional directional control valve	Valve function: 5/3-way Input: -5 ~ 5 V
Optical encoder	Decoder IC: HCTL-2032 Resolution: 20 nm
PC-based controller	Pentium III CPU RAM: 512 MB
A/D D/A cards	12 bit A/D × 16 CH 12 bit D/A × 6 CH D/I, D/O × 16 CH

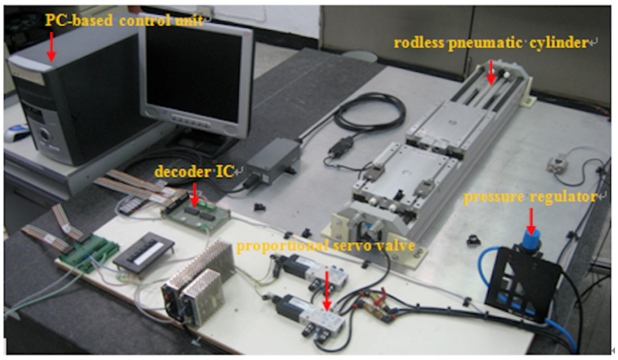

Fig. 2. Test rig of pneumatic actuator system.

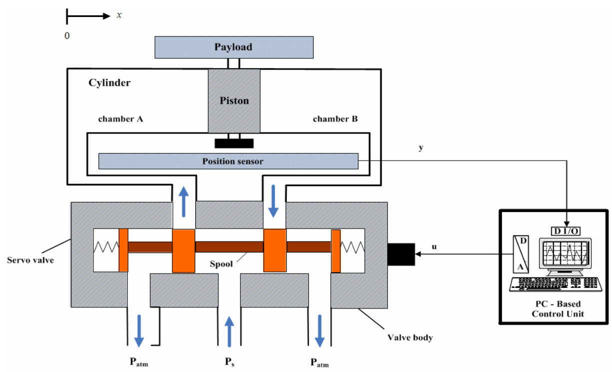

Fig. 3. Schematic drawing of a pneumatic actuator.

2.2 Pneumatic actuator system dynamic model

Fig. 2 shows the test rig of the PAS. In the rodless pneumatic servo system, the opening area of the proportional directional control valve's orifice depends on the control input to affect the air flow. As the air flows into the rodless pneumatic cylinder, the pressure difference between two cylinder chambers results in the motion of the pneumatic cylinder. An analysis of the dynamic behavior of the PAS usually requires individual mathematical descriptions of the dynamics of the three component parts: the valve, the actuator and the load. Such an analysis is presented below with reference to the coordinate system illustrated in Fig. 3.

2.2.1 Flow relationships for the control valves

With the assumption of constant supply and exhaust pressures, the mass flow rates m across two control ports of the control valves can be regarded as a function of the valve displacement and the chamber pressure [42, 43]

$$m_a = q_a(X, P_a), \tag{1}$$
$$m_b = q_b(X, P_b), \tag{2}$$

where m_a and m_b are the mass flow rates into the chambers A and B, X is the spool displacement of valves, P_a and P_b are the absolute pressures in the chambers A and B . According to the standard orifice theory, the mass flow rate through the valve orifice takes the form

$$m = \frac{C_d C_0 w X P_u \tilde{f}(p_r)}{T_u^{\frac{1}{2}}}, \tag{3}$$

where C_d is the discharge coefficient (C_d = 0.8), C_0 is the flow constant, w is the port width (m), T_u is the up-stream temperature, $p_r = P_d / P_u$ is the ratio between the down-stream and up-stream pressure at the orifice and

$$\tilde{f}(p_r) = \begin{cases} 1, & \dfrac{P_{atm}}{P_u} < p_r < C_r \\ C_k\left[p_r^{\frac{2}{k}} - p_r^{\frac{(k+1)}{k}}\right]^{\frac{1}{2}}, & C_r < p_r < 1 \end{cases}. \tag{4}$$

For air k = 1.4, C_r = 0.528 and C_k = 3.864. It can be shown that the function $\tilde{f}(\cdot)$ and its derivative are continuous with respect to p_r. For the convenience of the analysis, the following functions are introduced:

$$\hat{f}(P_a, P_s, P_e) = \begin{cases} \dfrac{P_s \tilde{f}(\frac{P_a}{P_s})}{\sqrt{T_s}} & \text{chamber A is a drive chamber} \\ \dfrac{P_a \tilde{f}(\frac{P_e}{P_a})}{\sqrt{T_a}} & \text{chamber B is a drive chamber} \end{cases}, \tag{5}$$

and

$$\hat{f}(P_b, P_s, P_e) = \begin{cases} \dfrac{P_b \tilde{f}(\frac{P_e}{P_b})}{\sqrt{T_b}} & \text{chamber A is a drive chamber} \\ \dfrac{P_s \tilde{f}(\frac{P_b}{P_s})}{\sqrt{T_s}} & \text{chamber B is a drive chamber} \end{cases}, \tag{6}$$

where $P_s = 6\times10^5$ Pa is the supply pressure, $P_e = 1\times10^5$ Pa is the exhaust pressure, T_s = 293 K is the cylinder air temperature, T_a and T_b are the temperatures of chambers A and B, respectively.

2.2.2 Dynamic relationship within the control chambers

From Refs. [42, 43], a model for the mass flow into each of the cylinder chambers can be obtained from the energy conservation equation for the control volume bounded by the cylinder and piston. The control volume energy is given by $c_V \rho_C V T_s$, where V is the cylinder volume, ρ_C is the cylinder air density and c_V is the specific heat of air at constant volume. If the air flows into the cylinder it is assumed to be an adiabatic process of a perfect gas, the change in energy due to the mass transport equals

$$\frac{d}{dt}\left(c_V \rho_C V T_s\right) = \dot{m} C_P T_s - P\dot{V}, \tag{7}$$

where C_P is the specific heat of air at a constant pressure, P is the cylinder chamber pressure, $mC_P T_s$ is the change in internal gas energy and $P\dot{V}$ is the work done by the cylinder. Assuming an ideal gas, $P = R\rho_C T_s$ and ρ_C can be eliminated in Eq. (7) to obtain

$$\begin{aligned} \dot{m} &= \frac{P}{C_P T_s}\frac{dV}{dt} + \frac{1}{kRT_s}\frac{d}{dt}\left(PV\right) \\ &= \frac{P}{C_P T_s}\dot{V} + \frac{1}{kRT_s}\dot{P}V + \frac{1}{kRT_s}P\dot{V}, \end{aligned} \tag{8}$$

where $k = \dfrac{C_P}{c_V}$ is the ratio of specific heats for air at the temperature T_s. For a perfect gas

$$\frac{1}{R} = \frac{1}{C_P} + \frac{1}{kR}, \tag{9}$$

then

$$\begin{aligned} \dot{m} &= \left(\frac{1}{C_P} + \frac{1}{kR}\right)\frac{1}{T_s}P\dot{V} + \frac{1}{kRT_s}\dot{P}V \\ &= \frac{1}{RT_s}P\dot{V} + \frac{1}{kRT_s}\dot{P}V. \end{aligned} \tag{10}$$

For the cylinder chambers A and B, the following equations hold:

$$\dot{m}_a = \frac{1}{RT_s}\left(P_a\dot{V}_a + \frac{V_a\dot{P}_a}{k}\right), \tag{11}$$

and

$$\dot{m}_b = \frac{1}{RT_s}\left(P_b\dot{V}_b + \frac{V_b\dot{P}_b}{k}\right). \tag{12}$$

From Eqs. (3)-(6), (11) and (12), the following equations can be derived:

$$\dot{P}_a = -\frac{k\dot{V}_a}{V_a}P_a + \frac{k}{V_a}RT_sC_dC_0wXf(P_a,P_s,P_e), \tag{13}$$

$$\dot{P}_b = -\frac{k\dot{V}_b}{V_b}P_b + \frac{k}{V_b}RT_sC_dC_0wXf(P_b,P_s,P_e), \tag{14}$$

where V_a and V_b are the volumes of chambers A and B, respectively.

2.2.3 Load dynamics

The moving mass, M, consists of the masses of the payload, the slide table and the piston. The force on the piston due to the air pressure and external load is expressed by

$$F_p = A(P_a - P_b) + F_l, \tag{15}$$

where F_l is external load force. The friction force is assumed to be modeled by the traditional combination of the stick-slip, Coulomb and viscous components. According to Newton's second law of motion, the pneumatic cylinder's motion can be described

$$F_p - F_r = M\ddot{x}. \tag{16}$$

The term F_r in Eq. (16) represents the sum of static and dynamic friction forces in the system, in which the static friction forces are unevenly distributed along the cylinders. This uneven distribution of friction causes difficulties for modeling and controlling the pneumatic cylinder actuators. The static component allows for stick-slip motion, as shown in Eq. (17).

$$F_r = \begin{cases} F_p, & \dot{x}=0 \ \ and \ \ |F_p| \le F_{sf} \\ F_{sf}, & \dot{x}=0 \ \ and \ \ |F_p| > F_{sf} \\ F_{cf} + K_{vf}\dot{x} & \dot{x} > 0 \\ -F_{cf} + K_{vf}\dot{x} & \dot{x} > 0 \end{cases} \tag{17}$$

where F_{sf} is the stick-slip friction force, F_{cf} is the Coulomb friction force, and K_{vf} is the coefficient of viscous friction. Further analysis and description of the static and the dynamic friction forces can be found in Refs. [44, 45].

The chamber volumes V_a and V_b are defined as

$$V_a = Ax + \overline{\Delta}, \tag{18}$$

$$V_b = A\left(l - x\right) + \overline{\Delta}, \tag{19}$$

where $\overline{\Delta}$ is the residual volume generated by the connecting tubes and components, l (m) is the stroke and $x \in [0,l]$. By rearranging Eqs. (18) and (19), the chambers volumes V_a and V_b can be rewritten as

$$V_a = A(x + \Delta), \tag{20}$$

$$V_b = A\left(l - x + \Delta\right), \tag{21}$$

where Δ can be considered as an equivalent extra length to the cylinder. Let $x_1 = x$, $x_2 = \dot{x}$, $x_3 = P_a$, $x_4 = P_b$, $u = X$, then a state-space system model is obtained

$$\dot{x}_1 = x_2, \tag{22a}$$

$$\dot{x}_2 = \frac{1}{M}\left[A(x_3 - x_4) + F_l - F_r\right], \tag{22b}$$

$$\dot{x}_3 = \frac{-k\left[x_2x_3 - \frac{RT_S}{A}C_dC_0w\hat{f}(x_3,P_s,P_e)u\right]}{x_1 + \Delta}, \tag{22c}$$

$$\dot{x}_4 = \frac{k\left[x_2x_4 - \frac{RT_S}{A}C_dC_0w\hat{f}(x_4,P_s,P_e)u\right]}{l - x_1 + \Delta}, \tag{22d}$$

where $x_1 \in \left[0,\ l\right]$, $x_3 \in \left[P_{e,}\ P_S\right]$, $x_4 \in \left[P_{e,}\ P_S\right]$. The system modeled by Eq. (22) can be considered as a cascade connection of two nonlinear subsystems, Eqs. (22a) and (22b) for the first subsystem and Eqs. (22c) and (22d) for the second subsystem. The parameters and values used in the system model are listed below:

A : Piston area (m^2) ,
$C_d = 0.8$: Discharge coefficient,
C_0 : Flow constant,
Δ : The general residual chamber volume,
K_{vf} : Viscous frictional coefficient,
P_{atm} : Atmospheric pressure (Pa),
l : Stroke 9 (m) and $x \in [0,l]$,
p_r : Ratio between down and up-stream pressure,
$R = 287$: Universal gas constant $J/(kg \cdot K)$,
$P_e = 1\times10^5$: Exhaust pressure (Pa)
$P_s = 6\times10^5$: Supply pressure (Pa)
$T_s = 293$: Cylinder air temperature (K)
$k = 1.4$: Specific heat constant
V : Volume (m^3)
w : Port width (m)
M : Payload (kg)
P_u : Up-stream pressure (Pa)
P_d : Down-stream pressure (Pa)

3. Description of Fourier neural networks

The features of fault tolerance, parallelism, and adaptation suggest that NNs make good candidates for the control of nonlinear systems, and the NN [25, 46, 47] can present a complex nonlinear function. A compact matrix form is shown as Eq. (23).

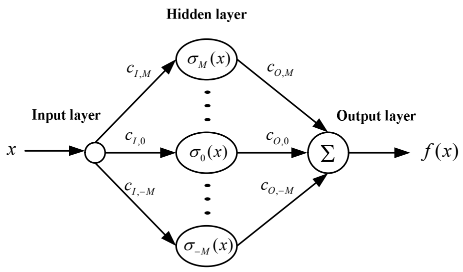

Fig. 4. Structure of a SISO FNN.

$$f(x) = \mathbf{W}^T \boldsymbol{\sigma}(x) + \varepsilon(x), \tag{23}$$

where $x \in \Re$ and $f \in \Re$ are the input and output, respectively, $\mathbf{W} = \begin{bmatrix} W_1 & \ldots & W_n \end{bmatrix}^T \in \Re^n$ is the network weight, $\boldsymbol{\sigma}(x) = \begin{bmatrix} \sigma_1(x) & \ldots & \sigma_n(x) \end{bmatrix}^T \in \Re^n$, $\sigma_i(\cdot), i = 1,2,...,n,$ denotes the activation function, and $\varepsilon(x)$ is called the NN function reconstruction error. If the structure, activation functions, and learning algorithm for Eq. (23) are chosen properly, the estimation error $\varepsilon(x)$ can be as accurate as desired. Some inherent problems, however, restrict the traditional NNs to the real applications, such as the selection of the network structure, the convergent speed, the problem of local minimum and the stability analysis of the closed-loop system.

Many abstracts and general situations have adopted extended concept of Fourier analysis, which is particularly used to decompose a signal into its component frequencies with different amplitudes and phases. The FNN is proposed in the view of the Fourier analysis and the neural network theory, which instead of using common Gaussian functions or sigmoid functions, the activation function $\sigma_i(\cdot)$ is selected as the family of complex Fourier functions. Due to Fourier analysis's excellent performance in nonlinear function modeling and decomposition, unlike ordinary NN, that employing the Fourier basis function may result in much higher availability of rates of convergence for the approximation. The structure of a Single-input-single-output (SISO) FNN is illustrated in Fig. 4. Both the input layer and the output layer only have one node. Note that the chosen node number in the hidden layer tends to be based upon the system bandwidth. In Fig. 4, x and $f(x)$, respectively, represent the input and output; $\sigma_i(x)$ ($i = -M,...,M$) are the basis functions; $c_{I,i}$ and $c_{O,i}$ ($i = -M,...,M$) are the weights of FNN; M is a positive integer based upon the system bandwidth, and the total number of the hidden layer neurons is $n = 2M + 1$. Therefore, the output function of the FNN is shown as

$$f(x) = \sum_{i=-M}^{M} c_{O,i} e^{jw_i x}. \tag{24}$$

The family of complex Fourier functions $e^{jw_n x}$ has orthogonality, where j is the imaginary unit that meets $j^2 = -1$, $w_n = \dfrac{2n\pi}{T}$ is the nth harmonic of the function f with $n = 0, \pm1, \pm2, ..., \pm\text{M}$, and $e^{jw_n x} = \cos w_n x + i \sin w_n x$ is based on Euler's formula. In real implementation, Eq. (24) is often represented as the sine/cosine form

$$f(x) = \mathbf{W}^T \mathbf{q}(x) \tag{25}$$

where $\mathbf{q}(x) \equiv \begin{bmatrix} 1, & \cos w_1 x, & \sin w_1 x, ..., \cos w_M x, & \sin w_M x \end{bmatrix}^T$ is the family of activation functions, and $\mathbf{W} \equiv \begin{bmatrix} W_0 & W_1 & \ldots & W_{2M-1} & W_{2M} \end{bmatrix}^T$ is the vector of network weights. Substituting the activation function $\boldsymbol{\sigma}(x)$ by the orthogonal Fourier activation function $\mathbf{q}(x)$, we can rewrite Eq. (23) as

$$f(x) = \mathbf{W}^T \mathbf{q}(x) + \varepsilon_n(x) \tag{26}$$

where $\varepsilon_n(t)$, $n = 2M + 1$, shows the approximation error and satisfies

$$|\varepsilon_n| \leq \sum_{i>n} (|w_i| + |w_{i+1}|). \tag{27}$$

The term $\mathbf{W}^T \mathbf{q}(x)$ in Eq. (26) is well-known to give the best possible mean square approximation to the function $f(x)$ [48]. The approximation error $\varepsilon_n(t)$ disappears as $n \to \infty$. Hence, $f(x)$ can be approximated as follows as long as n is large enough, with an error satisfying Eq. (27):

$$f(x) \cong \mathbf{W}^T \mathbf{q}(x). \tag{28}$$

FNN can be regarded as a particular case of NN. It maintains the same universal approximation property as a Fourier series and provides a specific link between the network coefficients and the Fourier transform. The nature of the ideal network weights of the FNN is the spectra of the approximated function. This clear physical picture indicates that when we employ the FNN in real applications, the selection of the term number M can be established on the system bandwidth. Thus, FNN can accomplish the same quality of approximation with a network of reduced size. Remark 1 expresses the idea of which the Fourier series is applied to approximate the non-periodic nonlinear functions.

Remark 1 [39]: Take into account of a nonlinear function $f(t)$ as a non-periodical function. We come to

$$f(t) = \int_{-\infty}^{\infty} F(w) e^{jwt} dw, \tag{29}$$

where $F(w) = \int_{-\infty}^{\infty} f(t) e^{-jwt} dt$. By applying Shannon's theory in the frequency domain, Eq. (29) is equivalent to partition the non-periodical function with an appropriate window in the time domain. Then, it can be achieved in discrete form,

$$f(t) = \int_{-\infty}^{\infty} F(w) e^{jwt} dw = \sum_{n=-M}^{M} X(n\Omega) e^{jn\Omega t} \Delta w, \tag{30}$$

where $\Omega = \dfrac{w_n}{n}$ is the base frequency acquired by discretizing

w. From an engineering point of view, the control objective is often defined at a limited time interval $[0,T]$, and consequently the base frequency can be simply selected as $\Delta w = \dfrac{2\pi}{T}$.

4. Design of control algorithms and stability analysis

The objective of this study was to develop an AFNN-based SMC with H_∞ tracking design technique for the motion control of a rodless PAS, in which the H_∞ tracking design technique is introduced in the SMC to handle the function approximation errors, un-modeled dynamics and disturbances. Before developing the controller, the feedback linearization should be done as in the following.

4.1 Feedback linearization of the input-output map

According to the proposed linearization strategy in Ref. [49], the model of PAS, as shown in Eq. (22), can be linearized by differentiating its output. The static and Coulomb friction forces as well as external load are considered as uncertainties so that we neglect it at the beginning while linearizing. By applying the feedback linearization theory to a pneumatic servo system Eq. (22), the system can be expressed as

$$\begin{aligned} \dot{\mathbf{x}} &= f(\mathbf{x},t) + g(\mathbf{x},t)u(t), \\ y &= h(\mathbf{x},t) = x_1, \end{aligned} \tag{31}$$

where the state vector $\mathbf{x}$ and control input u are

$$\mathbf{x} = \begin{bmatrix} x_1 \\ x_2 \\ x_3 \\ x_4 \end{bmatrix}, \quad u(t) = X, \tag{32}$$

and the corresponding vector field $f(\mathbf{x})$ and $g(\mathbf{x})$ are described as

$$f(\mathbf{x},t) = \begin{bmatrix} x_2 \\ \dfrac{1}{M}\left[-K_{vf}x_2 + A(x_3 - x_4)\right] \\ \dfrac{-k(x_2 x_3)}{x_1 + \Delta} \\ \dfrac{k(x_2 x_4)}{l - x_1 + \Delta} \end{bmatrix}, \tag{33}$$

$$g(\mathbf{x},t) = \begin{bmatrix} 0 \\ 0 \\ \dfrac{kRT_S C_d C_0 w\hat{f}(x_3, P_s, P_e)}{A(x_1 + \Delta)} \\ \dfrac{-kRT_S C_d C_0 w\hat{f}(x_4, P_s, P_e)}{A(l - x_1 + \Delta)} \end{bmatrix}, \tag{34}$$

in which $f(\mathbf{x},t)$ and $g(\mathbf{x},t)$ are unknown and smooth vector functions on the set $\Omega \subset \Re^4$; $y = h(\mathbf{x},t) \in (0,l) \subset \Re$. Let $L_f h$ and $L_g h$ be the *Lie derivatives* of h with respect to f and g. Since $L_g L_f^k h(\mathbf{x},t) = 0$ for all $k < 3$, and $L_g L_f^k h(\mathbf{x},t) \neq 0$ for all $k \geq 3$ for all x(t), the relative degree of the system is 3. Then, we obtain [50]

$$\begin{aligned} y^{(3)} &= L_f^3 h(\mathbf{x},t) + L_g L_f^2 h(\mathbf{x},t)u(t) \\ &= \left\{ \frac{K_{vf}^2 x_2 - K_{vf} A(x_3 - x_4)}{M^2} - \frac{Akx_2[x_3(l - x_1 + \Delta) + x_4(x_1 + \Delta)]}{M(x_1 + \Delta)(l - x_1 + \Delta)} \right\} \\ &\quad + \left\{ \frac{kRT_s C_d C_0 w[\hat{f}(x_3, P_s, P_e)(l - x_1 + \Delta) + \hat{f}(x_4, P_s, P_e)(x_1 + \Delta)]}{M(x_1 + \Delta)(l - x_1 + \Delta)} \right\} u \\ &= \bar{f}(\mathbf{x},t) + \bar{g}(\mathbf{x},t)u(t), \end{aligned} \tag{35}$$

where

$$\bar{f}(\mathbf{x},t) = \frac{K_{vf}^2 x_2 - K_{vf} A(x_3 - x_4)}{M^2} - \frac{Akx_2[x_3(l - x_1 + \Delta) + x_4(x_1 + \Delta)]}{M(x_1 + \Delta)(l - x_1 + \Delta)}$$

and

$$\bar{g}(\mathbf{x},t) = \frac{kRT_s C_d C_0 w[\hat{f}(x_3, P_s, P_e)(l - x_1 + \Delta) + \hat{f}(x_4, P_s, P_e)(x_1 + \Delta)]}{M(x_1 + \Delta)(l - x_1 + \Delta)}.$$

In Eq. (35), y is the piston displacement, $\mathbf{x}$ is the state vector, $\bar{f}(\mathbf{x},t)$ is the function of state variables, $\bar{g}(\mathbf{x},t)$ is the control gain, and $u(t)$ is the control input voltage of the servo valve. Note that $\bar{f}(\mathbf{x},t)$ and $\bar{g}(\mathbf{x},t)$ are time-varying functions with unknown variation bound.

However, the nonlinear time-varying behavior with uncertain bounds of the system dynamics makes it difficult to obtain an accurate dynamic model for a model-based controller design. Therefore, the AFNN is proposed here to approximate the unknown functions $\bar{f}(\mathbf{x},t)$ (to be discussed later) and $\bar{g}(\mathbf{x},t)$ to dispose of model dependency. In addition, H_∞ tracking control is introduced to compensate the approximation error and thus improve the control performance and reduce the computational load.

4.2 Design of an AFNN-SMC

Transforming the system dynamics Eq. (35) into a general system, we have the following equation:

$$y^{(n)} = \bar{f}(\mathbf{x},t) + \bar{g}(\mathbf{x},t)u(t) + d(\mathbf{x},t) \tag{36}$$

where $\mathbf{x} = [y(t) \quad \dot{y}(t) \quad \ldots \quad y^{(n-1)}(t)]^T \in \Re^n$ is the state vector; $u(t) \in \Re$ and $y \in \Re$ are, respectively, the control input and system output; $d(\mathbf{x},t)$ denotes the external disturbance and the unmodeled static and Coulomb friction forces, $\bar{f}(\mathbf{x},t)$ and $\bar{g}(\mathbf{x},t)$ are unknown functions with time-varying parameter uncertainty. Without loss of generality, $\bar{g}(\mathbf{x},t)$ can be assumed to be strictly positive, i.e., $\bar{g}(\mathbf{x},t) \geq g^l > 0$. Assuming that the solution of the system exists and the order of the system is known, we can rewrite Eq. (36) as

$$y^{(n)} = F(\mathbf{x},t) + \bar{g}(\mathbf{x},t)u(t) \tag{37}$$

where $F(\mathbf{x},t) = \bar{f}(\mathbf{x},t) + d(\mathbf{x},t)$. Hence, with $F(\mathbf{x},t)$ and $\bar{g}(\mathbf{x},t)$ in Eq. (37) as unknown time-varying functions, we use AFNN to approximate them for the controller design in this study. The adaptive laws of the coefficient vector of network weight can be acquired from the Lyapunov stability theorem. We make the following assumption to obtain a generalized result.

Assumption: (i) The nonlinear system expressed in Eq. (31) has a relative degree of n, (ii) the control u appears linear with respect to $y^{(n)}$ and $\bar{g}(\mathbf{x},t) \neq 0$ for $\mathbf{x}$ in some controllable region U_c, and (iii) the internal dynamics of the system with the following AFNN-SMC are stable.

In our experimental system, the unknown time-varying functions $F(\mathbf{x},t)$ and $\bar{g}(\mathbf{x},t)$ in Eq. (37) are bounded because the design of tests rig and restricted control outputs $u \in [-5\text{V}, 5\text{V}]$ limit the states, the piston position x_1, the velocity of piston x_2, and the acceleration of piston x_3. Therefore $F(\mathbf{x},t)$ and $\bar{g}(\mathbf{x},t)$ meet the Dirichlet conditions, so they can be indicated by the FNN as shown in Eq. (26). Hence, we have

$$\begin{aligned} y^{(n)} &= (\mathbf{W}_F^T \mathbf{q}_F(t) + \varepsilon_F(t)) + (\mathbf{W}_{\bar{g}}^T \mathbf{q}_{\bar{g}}(t) + \varepsilon_{\bar{g}}(t))u \\ &= \mathbf{W}_F^T \mathbf{q}_F(t) + \mathbf{W}_{\bar{g}}^T \mathbf{q}_{\bar{g}}(t)u + w_t \end{aligned} \tag{38}$$

where $\mathbf{q}_F(t)$ and $\mathbf{q}_{\bar{g}}(t)$ are the family orthogonal Fourier activation function vector, $\mathbf{W}_F$ and $\mathbf{W}_{\bar{g}}$ are the coefficient vector of network weight, and $w_t = \varepsilon_F(t) + \varepsilon_{\bar{g}}(t)u$ is the lumped uncertainty. To facilitate the design process of the controller, the lumped uncertainty is generally assumed to have an upper bound.

Assumption: (iv) There exists a positive constant w_t^u, such that $|w_t| \leq w_t^u$.

As a well-known fact, the terms $\mathbf{W}_F^T \mathbf{q}_F$ and $\mathbf{W}_g^T \mathbf{q}_{\bar{g}}$ are anticipated to produce an optimal mean square approximation to the uncertain time-varying functions $F(\mathbf{x},t)$ and $\bar{g}(\mathbf{x},t)$, respectively. Under the assumptions (i)-(iv), then, we can force the system output, $y(t)$, to follow a given bounded reference signal $y_m(t)$. The output tracking error can be written as

$$e = y - y_m. \tag{39}$$

A switch surface can be defined as

$$s = a_1 e + a_2 \dot{e} + \ldots + a_n e^{(n-1)},\ a_n = 1 \tag{40}$$

where a_i are chosen such that $\sum_{i=1}^{n} a_i \lambda^{i-1}$ is a Hurwitz polynomial in which λ is a Laplace operator. Eq. (40) indicates that

$$e^{(n-1)} = -a_1 e - a_2 \dot{e} - \ldots - a_{n-1} e^{(n-2)} + s. \tag{41}$$

If $\mathbf{e} = [e, \dot{e}, \ldots, e^{(n-2)}]^T = [e_1, e_2, \ldots, e_{n-1}]^T$, the error dynamics will become

$$\dot{\mathbf{e}} = \mathbf{A}_1 \mathbf{e} + [0, \ldots, 0, s]^{\mathbf{T}} \tag{42}$$

where $\mathbf{A}_1 = \begin{bmatrix} 0 & 1 & 0 & \cdots & 0 \\ 0 & 0 & 1 & \cdots & 0 \\ \vdots & \vdots & \vdots & \ddots & \vdots \\ -a_1 & -a_2 & -a_3 & \cdots & -a_{n-1} \end{bmatrix}$.

Theorem 1: Take the finite bandwidth system into account with unknown nonlinear time-varying functions $F(\mathbf{x},t)$ and $\bar{g}(\mathbf{x},t)$ in Eq. (37), which is approximated as Eq. (28). Suppose assumptions (i)-(iv) are satisfied and following similar derivations in Refs. [32, 51], we can acquire a control law for Eq. (38) by applying the sliding-mode control method, the control input is chosen as

$$u = \frac{-\hat{\mathbf{W}}_F^T \mathbf{q}_F(t) - \sum_{i=1}^{n-1} a_i e_{i+1} - \sum_{i=1}^{n-1} p_{(n-1)i} e_i + y_m^{(n)} - k_p \operatorname{sgn}(s)}{\hat{\mathbf{W}}_{\bar{g}}^T \mathbf{q}_{\bar{g}}(t)} \tag{43}$$

where $\hat{\mathbf{W}}_F^T$ and $\hat{\mathbf{W}}_{\bar{g}}^T$ are the estimates of $\mathbf{W}_F^T$ and $\mathbf{W}_{\bar{g}}^T$, respectively. Choosing $\mathbf{P} > 0,\ \mathbf{P} \in R^{(n-1)\times(n-1)}$, satisfies the Lyapunov matrix equation

$$\mathbf{A}_1^{\mathbf{T}} \mathbf{P} + \mathbf{P} \mathbf{A}_1 = -\mathbf{Q} \tag{44}$$

with s being the sliding surface defined in Eq. (40); $p_{(n-1)i}$ being elements of $\mathbf{P}$ in Eq. (44); $\mathbf{Q} > 0$ being given and the adaptive laws being chosen as

$$\begin{aligned} \dot{\hat{\mathbf{W}}}_F &= \mathbf{\Gamma}_1 s \mathbf{q}_F(t) \\ \dot{\hat{\mathbf{W}}}_{\bar{g}} &= \mathbf{\Gamma}_2 s \mathbf{q}_{\bar{g}}(t) u \end{aligned} \tag{45}$$

where $\mathbf{\Gamma}_1$ and $\mathbf{\Gamma}_2$ ($\mathbf{\Gamma}_1 > 0$ and $\mathbf{\Gamma}_2 > 0$) are the adaptation gain matrix, the following result holds for s and $\mathbf{e}$: $s \to 0$ and $\mathbf{e} \to 0$ as $t \to \infty$.

Proof:

Suppose the Lyapunov function as

$$\mathrm{V} = \frac{1}{2}s^2 + \frac{1}{2}\mathbf{e}^{\mathbf{T}} \mathbf{P} \mathbf{e} + \frac{1}{2}\tilde{\mathbf{W}}_F^T \mathbf{\Gamma}_1^{-1} \tilde{\mathbf{W}}_F + \frac{1}{2}\tilde{\mathbf{W}}_{\bar{g}}^T \mathbf{\Gamma}_2^{-1} \tilde{\mathbf{W}}_{\bar{g}} \tag{46}$$

where $\tilde{\mathbf{W}}_F = \mathbf{W}_F - \hat{\mathbf{W}}_F$, and $\tilde{\mathbf{W}}_{\bar{g}} = \mathbf{W}_{\bar{g}} - \hat{\mathbf{W}}_{\bar{g}}$. The time derivative of Eq. (46) becomes

$$\begin{aligned}
\dot{V} &= s\dot{s} + \frac{1}{2}\dot{\mathbf{e}}^{\mathrm{T}}\mathbf{P}\mathbf{e} + \frac{1}{2}\mathbf{e}^{\mathrm{T}}\mathbf{P}\dot{\mathbf{e}} + \tilde{\mathbf{W}}_F^T\mathbf{\Gamma}_1^{-1}\dot{\tilde{\mathbf{W}}}_F + \tilde{\mathbf{W}}_{\bar{g}}^T\mathbf{\Gamma}_2^{-1}\dot{\tilde{\mathbf{W}}}_{\bar{g}} \\
&= s\dot{s} + \frac{1}{2}\left[\mathbf{e}^{\mathrm{T}}\mathbf{A}_1^{\mathrm{T}} + [0,...,0,s]\right]\mathbf{P}\mathbf{e} + \frac{1}{2}\mathbf{e}^{\mathrm{T}}\mathbf{P}\left[\mathbf{A}_1\mathbf{e} + [0,...,0,s]^T\right] \\
&\quad -\tilde{\mathbf{W}}_F^T\mathbf{\Gamma}_1^{-1}\dot{\hat{\mathbf{W}}}_F - \tilde{\mathbf{W}}_{\bar{g}}^T\mathbf{\Gamma}_2^{-1}\dot{\hat{\mathbf{W}}}_{\bar{g}} = s\left[e^{(n)} + a_{n-1}e^{(n-1)} + ... + a_1\dot{e}\right] \\
&\quad -\frac{1}{2}\mathbf{e}^{\mathrm{T}}\mathbf{Q}\mathbf{e} + \frac{1}{2}[0,...,0,s]\mathbf{P}\mathbf{e} + \frac{1}{2}\mathbf{e}^{\mathrm{T}}\mathbf{P}[0,...,0,s]^{\mathrm{T}} - \tilde{\mathbf{W}}_F^T\mathbf{\Gamma}_1^{-1}\dot{\hat{\mathbf{W}}}_F \\
&\quad -\tilde{\mathbf{W}}_{\bar{g}}^T\mathbf{\Gamma}_2^{-1}\dot{\hat{\mathbf{W}}}_{\bar{g}} = s\left[y^{(n)} - y_m^{(n)} + a_{n-1}e_n + ... + a_1e_2\right] - \frac{1}{2}\mathbf{e}^{\mathrm{T}}\mathbf{Q}\mathbf{e} \\
&\quad +[0,...,0,s]\mathbf{P}\mathbf{e} - \tilde{\mathbf{W}}_F^T\mathbf{\Gamma}_1^{-1}\dot{\hat{\mathbf{W}}}_F - \tilde{\mathbf{W}}_{\bar{g}}^T\mathbf{\Gamma}_2^{-1}\dot{\hat{\mathbf{W}}}_{\bar{g}} \\
&= s\left[F(\mathbf{x},t) + \bar{g}(\mathbf{x},t)u - y_m^{(n)} + a_{n-1}e_n + ... + a_1e_2\right] \\
&\quad -\frac{1}{2}\mathbf{e}^{\mathrm{T}}\mathbf{Q}\mathbf{e} + s\sum_{i=1}^{n-1}p_{(n-1)i}e_i - \tilde{\mathbf{W}}_F^T\mathbf{\Gamma}_1^{-1}\dot{\hat{\mathbf{W}}}_F - \tilde{\mathbf{W}}_{\bar{g}}^T\mathbf{\Gamma}_2^{-1}\dot{\hat{\mathbf{W}}}_{\bar{g}} \\
&= s\left[\mathbf{W}_F^T\mathbf{q}_F(t) + \mathbf{W}_{\bar{g}}^T\mathbf{q}_{\bar{g}}(t)u + w_t - y_m^{(n)} + \sum_{i=1}^{n-1}a_ie_{i+1}\right] \\
&\quad -\frac{1}{2}\mathbf{e}^{\mathrm{T}}\mathbf{Q}\mathbf{e} + s\sum_{i=1}^{n-1}p_{(n-1)i}e_i - \tilde{\mathbf{W}}_F^T\mathbf{\Gamma}_1^{-1}\dot{\hat{\mathbf{W}}}_F - \tilde{\mathbf{W}}_{\bar{g}}^T\mathbf{\Gamma}_2^{-1}\dot{\hat{\mathbf{W}}}_{\bar{g}} \\
&= s\left[(\tilde{\mathbf{W}}_F^T + \hat{\mathbf{W}}_F^T)\mathbf{q}_F(t) + (\tilde{\mathbf{W}}_{\bar{g}}^T + \hat{\mathbf{W}}_{\bar{g}}^T)\mathbf{q}_{\bar{g}}(t)u + w_t \right.\\
&\quad \left. -y_m^{(n)} + \sum_{i=1}^{n-1}a_ie_{i+1}\right] \\
&\quad -\frac{1}{2}\mathbf{e}^{\mathrm{T}}\mathbf{Q}\mathbf{e} + s\sum_{i=1}^{n-1}p_{(n-1)i}e_i - \tilde{\mathbf{W}}_F^T\mathbf{\Gamma}_1^{-1}\dot{\hat{\mathbf{W}}}_F - \tilde{\mathbf{W}}_{\bar{g}}^T\mathbf{\Gamma}_2^{-1}\dot{\hat{\mathbf{W}}}_{\bar{g}} \\
&= s[\hat{\mathbf{W}}_F^T\mathbf{q}_F(\mathbf{x}) + \hat{\mathbf{W}}_{\bar{g}}^T\mathbf{q}_{\bar{g}}(t)u + w_t - y_m^{(n)} + \sum_{i=1}^{n-1}a_ie_{i+1}] - \frac{1}{2}\mathbf{e}^{\mathrm{T}}\mathbf{Q}\mathbf{e} \\
&\quad +s\sum_{i=1}^{n-1}p_{(n-1)i}e_i + \tilde{\mathbf{W}}_F^T(s\mathbf{q}_F(t) - \mathbf{\Gamma}_1^{-1}\dot{\hat{\mathbf{W}}}_F) + \tilde{\mathbf{W}}_{\bar{g}}^T(s\mathbf{q}_{\bar{g}}(t)u - \mathbf{\Gamma}_2^{-1}\dot{\hat{\mathbf{W}}}_{\bar{g}}).
\end{aligned} \tag{47}$$

Applying Eqs. (43) and (45)-(47) and letting $k_p = k_1 + w_t^u$, $k_1 > 0$, we get the following relationship:

$$\dot{V} \le -k_p|s| - \frac{1}{2}\mathbf{e}^{\mathrm{T}}\mathbf{Q}\mathbf{e} + sw_t \le -k_1|s| - \frac{1}{2}\mathbf{e}^{\mathrm{T}}\mathbf{Q}\mathbf{e} \le 0. \tag{48}$$

According to Barbalat's lemma, Eq. (48) suggests that when $t \to \infty$, $s \to 0$ then $\mathbf{e} \to 0$.

Remark 2: In this algorithm, the AFNN approximates the system unknown nonlinear time-varying functions, and an adaptive control law is employed to adjust the network weights to improve the convergence speed. Whenever there is an error, the compensating term $k_p\,\mathrm{sgn}(s)$ is used to guarantee the closed-loop asymptotic stabilization and convergence of the overall system. Because the network can automatically adjust its weighting values, an effective adaptation is achieved for practical control applications.

4.3 H_∞ tracking performance design

To reduce the adverse effects resulting from approximate errors, un-modeled dynamics and disturbances prior, we combine the technique of H_∞ tracking design and the AFNN approximation with the sliding mode control method. To put it into practice, however, the exact upper bound w_t^u for the lumped uncertainty cannot be obtained in general. Given that the upper bound w_t^u can be chosen so as to attenuate the lumped uncertainty, large control chattering nevertheless occurs. To release the constraint of $k_p > w_t^u$, a new control law developed from the H_∞ tracking design technique is proposed. According to the assumption of which the lumped uncertainty is $w_t \in L_2[0,T]$, $\forall T \in [0,\infty)$ [32], the control input can be shown as

$$u = \frac{-\hat{\mathbf{W}}_F^T\mathbf{q}_F(t) - \sum_{i=1}^{n-1}a_ie_{i+1} - \sum_{i=1}^{n-1}p_{(n-1)i}e_i + y_m^{(n)} - \dfrac{s}{2\rho^2}}{\hat{\mathbf{W}}_{\bar{g}}^T\mathbf{q}_{\bar{g}}(t)}. \tag{49}$$

In Eq. (49), the adaptive laws can be represented as Eq. (45) with ρ ($\rho > 0$) being the design constant for the attenuation level, s being the sliding surface defined in Eq. (40) and $p_{(n-1)i}$ being elements of $\mathbf{P}$ in Eq. (44). Therefore, we can guarantee an H_∞ tracking performance for overall without knowledge on the upper bound w_t^u of the lumped uncertainty.

Theorem 2: Under assumptions (i)-(iii), the proposed control law Eq. (49) ensures that the overall system Eq. (22) satisfies the H_∞ tracking performance.

$$\begin{aligned}
&\frac{1}{2}\int_0^T \mathbf{e}^T(\tau)\mathbf{Q}\mathbf{e}(\tau)d\tau \le \frac{1}{2}s^2(0) + \frac{1}{2}\mathbf{e}^T(0)\mathbf{P}\mathbf{e}(0) \\
&+\frac{1}{2}\tilde{\mathbf{W}}_g^T(0)\mathbf{\Gamma}_2^{-1}\tilde{\mathbf{W}}_g(0) + \frac{1}{2}\rho^2\frac{1}{2}\int_0^T w_t^2(\tau)d\tau
\end{aligned} \tag{50}$$

where $\tilde{\mathbf{W}}_F = \mathbf{W}_F - \hat{\mathbf{W}}_F$ and $\tilde{\mathbf{W}}_g = \mathbf{W}_g - \hat{\mathbf{W}}_g$.

Proof:

Select the same Lyapunov function as Eq. (46) in accordance with the same procedure of Eq. (47). Then substituting Eqs. (45) and (49) into Eq. (47), we get

$$\dot{V} = -\frac{1}{2}\mathbf{e}^{\mathrm{T}}\mathbf{Q}\mathbf{e} - \frac{1}{2}\left(\frac{s}{\rho} - \rho w_t\right)^2 + \frac{1}{2}\rho^2w_t^2 \le -\frac{1}{2}\mathbf{e}^{\mathrm{T}}\mathbf{Q}\mathbf{e} + \frac{1}{2}\rho^2w_t^2. \tag{51}$$

Integrating Eq. (51) from $t = 0$ to $t = T$, we obtain

$$\begin{aligned}
&\int_0^T \dot{V}(\tau)d\tau \le -\frac{1}{2}\int_0^T \mathbf{e}^{\mathrm{T}}(\tau)\mathbf{Q}\mathbf{e}(\tau)d\tau + \frac{1}{2}\rho^2\int_0^T w_t^2d\tau \\
&\Rightarrow V(T) - V(0) \le -\frac{1}{2}\int_0^T \mathbf{e}^{\mathrm{T}}(\tau)\mathbf{Q}\mathbf{e}(\tau)d\tau + \frac{1}{2}\rho^2\int_0^T w_t^2d\tau \\
&\Rightarrow 0 \le V(T) \le V(0) - \frac{1}{2}\int_0^T \mathbf{e}^{\mathrm{T}}(\tau)\mathbf{Q}\mathbf{e}(\tau)d\tau + \frac{1}{2}\rho^2\int_0^T w_t^2d\tau \\
&\Rightarrow 0 \le V(0) - \frac{1}{2}\int_0^T \mathbf{e}^{\mathrm{T}}(\tau)\mathbf{Q}\mathbf{e}(\tau)d\tau + \frac{1}{2}\rho^2\int_0^T w_t^2d\tau \\
&\Rightarrow \frac{1}{2}\int_0^T \mathbf{e}^{\mathrm{T}}(\tau)\mathbf{Q}\mathbf{e}(\tau)d\tau \le V(0) + \frac{1}{2}\rho^2\int_0^T w_t^2d\tau.
\end{aligned} \tag{52}$$

Substituting Eq. (46) into Eq. (52), we achieve a H_∞

tracking performance satisfying:

$$\frac{1}{2}\int_0^T \mathbf{e}^{\mathrm{T}}(\tau)\mathbf{Q}\mathbf{e}(\tau)d\tau \le \frac{1}{2}s^2(0)+\frac{1}{2}\mathbf{e}^{\mathrm{T}}(0)\mathbf{P}\mathbf{e}(0)+\frac{1}{2}\tilde{\mathbf{W}}_F^T(0)\mathbf{\Gamma}_1^{-1}\tilde{\mathbf{W}}_F(0)$$
$$+\frac{1}{2}\tilde{\mathbf{W}}_g^T(0)\mathbf{\Gamma}_2^{-1}\tilde{\mathbf{W}}_g(0)+\frac{1}{2}\rho^2\int_0^T w_t^{\,2}d\tau. \qquad (53)$$

Therefore, the H_∞ tracking performance is achieved with a prescribed. This completes the proof.

In Theorem 2, if the design constant, ρ, serving as an attenuation level, needs to be pre-specified during the design process, the constraint on setting an upper bound w_t^u for the unknown lumped uncertainties in Eq. (43) is, thus, removed. Furthermore, the chattering effect of the control input is substantially reduced with this method because the term $k_p\,\mathrm{sgn}(s)$ related to the control chattering in Eq. (43) is replaced by a much smoother term $s/(2\rho^2)$ in the derived control law of Eq. (49).

Remark 3: If a set of the initial conditions of $\mathbf{e}$, s, $\mathbf{W}_F$ and $\mathbf{W}_{\bar{g}}$ ($\mathbf{e}(0)=0,\ s(0)=0,\ \hat{\mathbf{W}}_F(0)=\mathbf{W}_F(0)$ and $\hat{\mathbf{W}}_{\bar{g}}(0)=\mathbf{W}_{\bar{g}}(0)$) is available, and $\mathbf{Q}=\mathrm{I}$, the overall system's control performance satisfies

$$\frac{\|\mathbf{e}\|_2}{\|w_t\|_2} \le \rho, \qquad (54)$$

where $\|\mathbf{e}\|_2^2=\int_0^T \mathbf{e}^T(\tau)\mathbf{e}(\tau)d\tau,\ \|w_t\|_2^2=\int_0^T w_t^{\,2}(\tau)d\tau$. In other words, an arbitrary attenuation level can be obtained, if ρ is adequately chosen.

In real applications, the implementation of the AFNN-SMC+H-infinity algorithm, in general, can be formed by sine/cosine function. The detailed steps are presented here.

Step 1) Select control parameters $a_1, a_2, ..., a_{n-1}$ such that matrix $\mathbf{A}_1$ is a Hurwitz matrix.

Step 2) Choose appropriate $\mathbf{Q}$ to solve the Lyapunov matrix Eq. (44).

Step 3) Refer to the system bandwidth to establish AFNN to approximate the uncertain nonlinear function $F(\mathbf{x},t)$ and $\bar{g}(\mathbf{x},t)$. Determine initial values of network weight $\hat{\mathbf{W}}_F$ and $\hat{\mathbf{W}}_{\bar{g}}$, respectively.

Step 4) Choose an appropriate adaptation gain matrix $\mathbf{\Gamma}_1$ and $\mathbf{\Gamma}_2$ to establish the Lyapunov function.

Step 5) Obtain the update laws from Eq. (45), and the control laws from Eq. (43) or Eq. (49), respectively, depending on different assumptions on the lumped uncertainties.

5. Real-time implementation and experimental results

The objective of this study was to implement an AFNN-based sliding-mode controller to improve the tracking performance for the PAS. To investigate the control performance of the proposed controller, we present the test results of tracking control and velocity control in a PAS. In the experimental

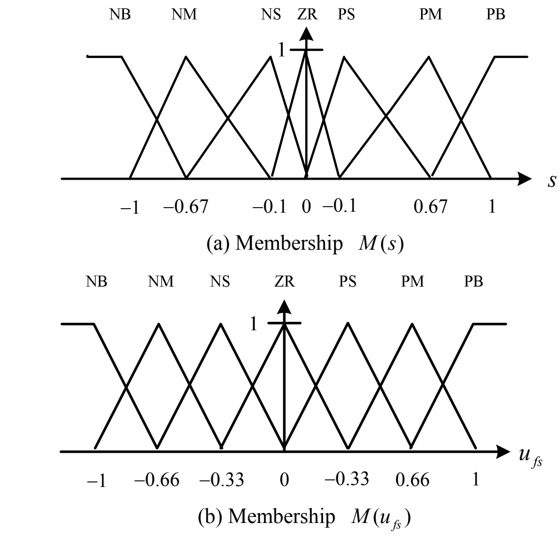

Fig. 5. Membership functions of the s and u_{fs}.

implementation, position regulation, trajectory tracking, and velocity control of the PAS are chosen for servo control. In addition, robustness tests are also performed to verify the proposed control strategy.

5.1 Experimental setup

To reduce the cost of the system set-up, the velocity and acceleration of the piston, as shown in Fig. 1, are calculated by a filtered differentiation of the measured position with a cut-off frequency at 350 Hz. The digital filter expressed is as follows:

$$y_{out}(i) = -0.047\,y_{out}(i-1) + 0.524[y_{in}(i) + y_{in}(i-1)], \qquad (55)$$

where $y_{out}(t)$ represents the filter's output signal, and $y_{in}(t)$ represents the measured piston position. To evaluate the control performance of the proposed AFNN-SMC+H_∞, the following experiments are performed. The attenuation level is set at $\rho = 0.2$ for the control law Eq. (48), the sliding surface is chosen as $s=\ddot{e}+2\dot{e}+6e$, $Q=\begin{bmatrix}1 & 2\\ 2 & 5\end{bmatrix}$, and the gain matrixes are set as constant matrices $\mathbf{\Gamma}_1 = 83\,[I]$ and $\mathbf{\Gamma}_2 = 1.25\times 10^{-4}[I]$.

To verify the feasibility, the Single-input fuzzy sliding mode controller (SFSMC), as proposed by Kim and Lee [53], was used to compare with the proposed AFNN-SMC and AFNN-SMC+H_∞ in terms of position regulation and trajectory tracking control performance. The sliding surface s and the control law u_{fs}, are, respectively, chosen as the input and output of SFSMC, and their membership functions are shown in Figs. 5(a) and (b). *NB*, *NM*, *NS*, *ZR*, *PS*, *PM*, and *PB*. In addition, the product inference, center-averaging, and singleton fuzzification are used in the fuzzy logic system. The

Table 2. Control parameters of SFSMC.

Sliding surface	g_s	g_u
$s=\dot{e}+12e$	0.2	0.8

Table 3. Rule table of the SFSMC.

Rule	Input variable s	Output variable u_{fs}
R_1	If s is PB	Then u_{fs} is PB
R_2	If s is PM	Then u_{fs} is PM
R_3	If s is PS	Then u_{fs} is PS
R_4	If s is ZR	Then u_{fs} is ZR
R_5	If s is NB	Then u_{fs} is NB
R_6	If s is NM	Then u_{fs} is NM
R_7	If s is NS	Then u_{fs} is NS

control parameters and the rule base of SFSMC are listed in Tables 2 and 3, respectively.

5.2 Test result of position regulation

The PAS plays an important role in industrial applications because it can easily and smoothly move a payload from one position to another. Hence, planning a smooth moving trajectory is vital. Moreover, because of the mechanical limitations, the maximum acceleration and velocity should be considered in the trajectory design. In our experiments, the fifth-order polynomial continuous function is adopted to be the moving trajectory, which is a trajectory function of the continuous displacement, the velocity and the acceleration [41], as shown in Eq. (56).

$$y_m(t)=\begin{cases} h\left[10\left(\dfrac{t}{t_f}\right)^3-15\left(\dfrac{t}{t_f}\right)^4+6\left(\dfrac{t}{t_f}\right)^5\right], & 0\le t<t_f \\ h, \ t_f\le t \end{cases} \tag{56}$$

where h is the desired stroke; t_f denotes the desired duration; y_m indicates the desired path and t is the time which is set to 0 at the beginning of each tracking cycle. Then, we can reduce discontinuous shock and wear-out and fatigue of the hardware components when the payload is moving.

For the position regulation, the piston is first moved to the end of the cylinder and this position is then assumed to be the original point $y(0)=0$ mm. In addition, the desired position is set to $y_d=150$ mm. A performance comparison between AFNN-SMC, SFSMC, and AFNN-SMC+ H_∞ is shown in Figs. 6-8. Figs. 6(b), 7(b) and 8(b) illustrate that the position errors of the three control methods are well converged and bounded with around ±1.8 mm (AFNN-SMC), ±2.2 mm (SFSMC), and ±0.9 mm (AFNN-SMC+ H_∞). Figs. 6(c), 7(c) and 8(c) show the steady errors of AFNN-SMC, SFSMC, and AFNN-SMC+ H_∞ are around 0.02 mm, 0.06 mm and

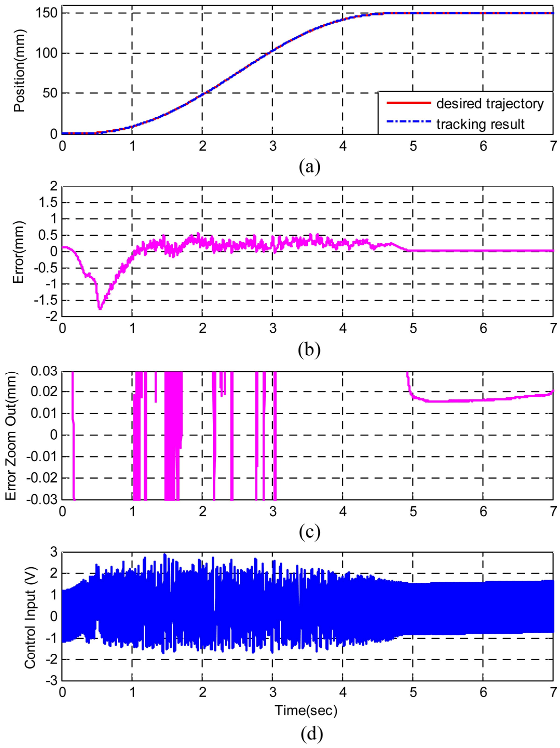

Fig. 6. Experimental results of AFNN-SMC for position regulation with position of 150 mm: (a) position control response; (b) control error; (c) error zoom out; (d) control input.

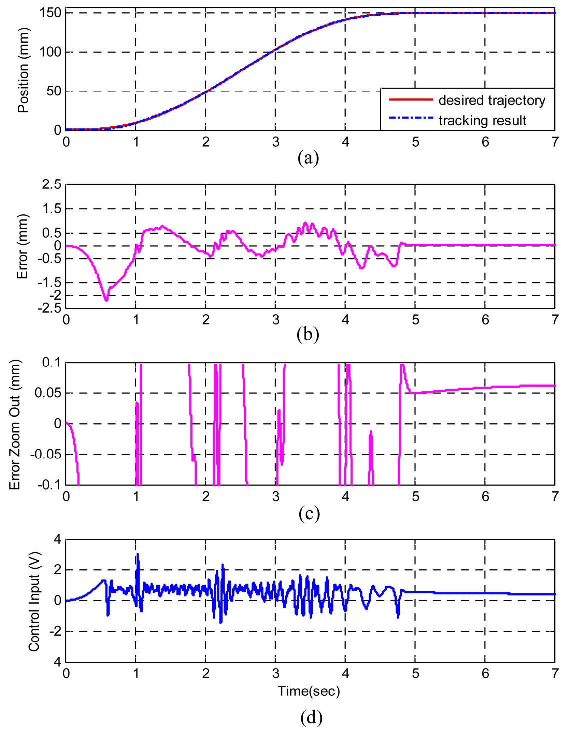

Fig. 7. Experimental results of SFSMC for position regulation with position of 150 mm: (a) position control response; (b) control error; (c) error zoom out; (d) control input.

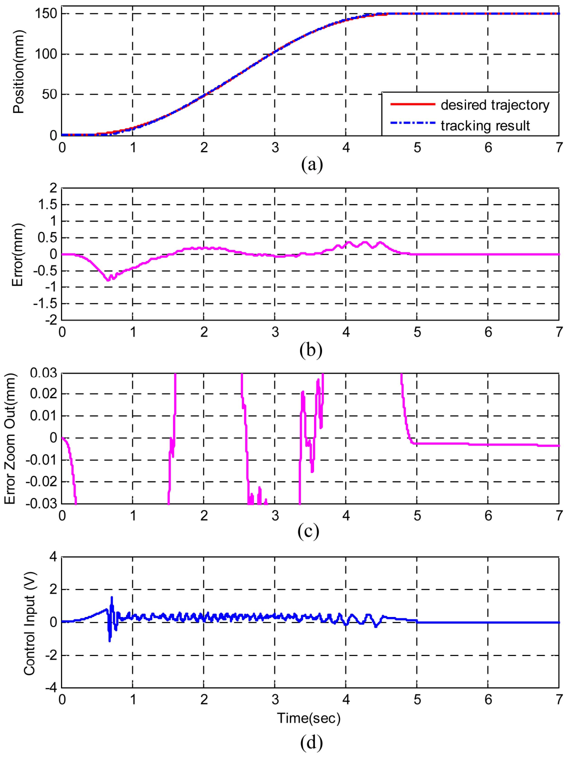

Fig. 8. Experimental results of AFNN-SMC+ H_∞ for position regulation with position of 150 mm: (a) position control response; (b) control error; (c) error zoom out; (d) control input.

0.04 mm, respectively. Observing the control input in Figs. 6(d), 7(d) and 8(d), we can find that the amplitude and chattering of AFNN-SMC are much worse than that of SFSMC and AFNN-SMC+ H_∞. That is because a bigger controller factor $k_p = 21000$ of AFNN-SMC is applied to the system to ensure the tracking performance. Note that the controller factor k_p of Eq. (43) is a trade-off parameter between the robustness and tracking performance. This undesired chattering may wear out the servo valve and can incur unstable system dynamics. In general, the term $k_p \operatorname{sgn}(s)$ in control law Eq. (43) is applied for compensating the lumped uncertainties, but it may result in serious control chattering. Moreover, although AFNN-SMC has better tracking effects and lower steady state error when compared with them with SFSMC, the effect of restricted chattering of SFSMC is much superior to it of AFNN-SMC, because of use of fuzzy design. Figs. 8(c) and (d) show that introducing H_∞ technique into AFNN-SMC (AFNN-SMC+ H_∞) can gain better tracking performance and chattering-reduction, as we compare it with AFNN-SMC and SFSMC. In Fig. 9, the integral time absolute error ITAE $= \int t|e(t)|dt$ is used to measure the tracking error of the position regulation for AFNN-SMC, SFSMC, and AFNN-SMC+ H_∞. It is obvious that the proposed AFNN-SMC+ H_∞ can perform much lower ITAE than others. Thus, the AFNN-

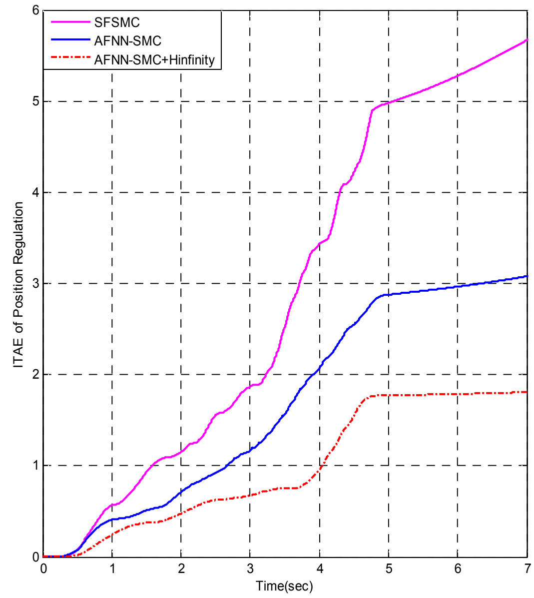

Fig. 9. Comparison of ITAE of tracking error for position regulation of AFNN-SMC, SFSMC and AFNN-SMC+ H_∞.

SMC+ H_∞ has superior control performance in controlling the PAS.

5.3 Test results of trajectory tracking

Case 1. Sinusoidal trajectory

The desired sinusoidal trajectory is defined as

$$y_m(t) = 50 + h\,[1 - \sin(t/T \cdot 2\pi)], \tag{57}$$

where the amplitude $h = 100$ mm and the period $T = 4$ sec are given in this paper. A comparison between AFNN-SMC, and SFSMC and AFNN-SMC+ H_∞ is shown in Figs. 10-12. From Figs. 10(b), 11(b) and 12(b), the tracking errors for those controllers are, respectively, around $\pm$ 1.8 mm, $\pm$ 2.0 mm, and $\pm$ 1.0 mm. Again, although the desired tracking performance of AFNN-SMC, as shown in Fig. 10(c), can be achieved, the chattering of the control input is still serious, which may result in high frequency switching of the servo valve and further reduce the servo valve's life duration. Compared to SFSMC with AFNN-SMC, as shown in Figs. 10 and 11, AFNN-SMC has better tracking effects and lower steady state error, but control chattering is very serious. That is, the SFSMC can effectively prevent chattering by using fuzzy approach. Fig. 12 shows the experimental results of AFNN-SMC+ H_∞ control, in which Fig. 12(a) shows the tracking response, where the dotted line indicates the target trajectory and the solid line denotes the tracking results. Fig. 12(b) shows the maximum tracking error is only about 1 mm, and Fig. 12(c) shows the control input, in which the chattering is significantly reduced. Compared to AFNN-SMC and SFSMC, AFNN-SMC+ H_∞ has better tracking performance and smooth control input.

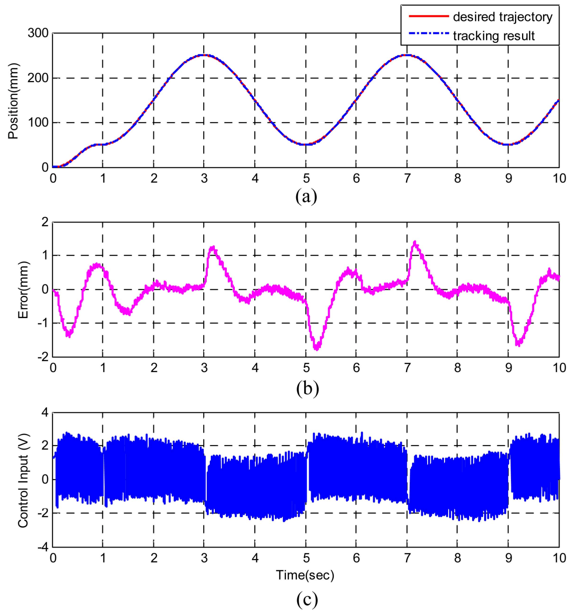

Fig. 10. Experimental results of AFNN-SMC for sinusoidal trajectory: (a) position control response; (b) control error; (c) control input.

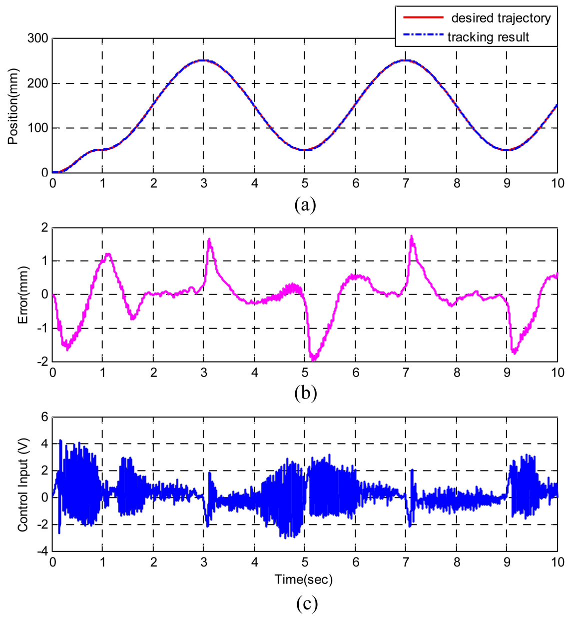

Fig. 11. Experimental results of SFSM for sinusoidal trajectory: (a) position control response; (b) control error; (c) control input.

Case 2. Exponentially decreasing sinusoidal trajectory

To verify the AFNN-SMC+ H_∞ control, we next test the performance of the exponentially decreasing 0.5 Hz sinusoidal trajectory covering 50% of the actuator stroke. The position responses, control efforts, and tracking errors, shown in Fig. 13, clarify that the AFNN-SMC+ H_∞ control can achieve excellent control performance with small chattering for the exponentially decreasing 0.5 Hz sinusoidal trajectory tracking control. Fig. 13(b) shows that the control error is bounded.

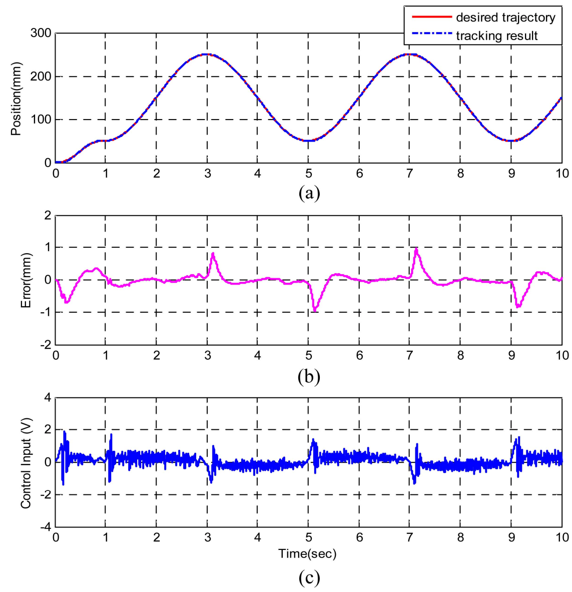

Fig. 12. Experimental results of AFNN-SMC+ H_∞ for sinusoidal trajectory: (a) position control response; (b) control error; (c) control input.

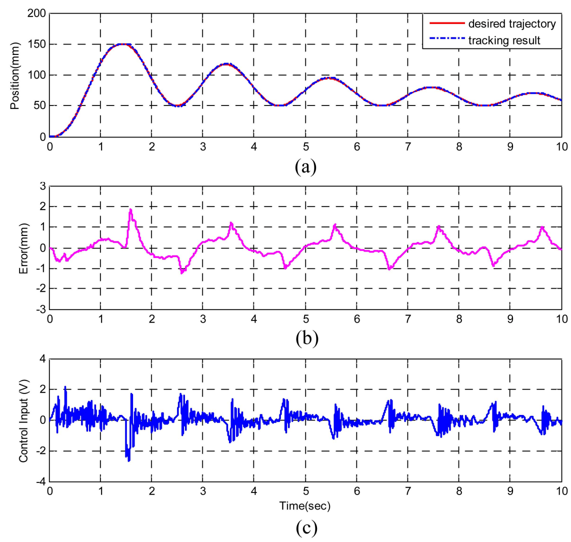

Fig. 13. Experimental results of AFNN-SMC+ H_∞ for exponentially decreasing sinusoidal trajectory: (a) position control response; (b) control error; (c) control input.

5.4 Test results of trapezoidal velocity trajectory

In most servo PASs the control purpose is expressed in terms of driving the cylinder piston to follow a predefined velocity profile to achieve the desired velocity control. In almost all industrial applications, a trapezoidal velocity profile is employed. For example, a constant velocity trajectory is required to apply paint or other coatings evenly across a surface. Another example would be to lay down a smooth bead when welding. The trapezoidal velocity profile consists of three distinct operating phases. The first phase is when the piston begins moving from rest and attains the desired velocity.

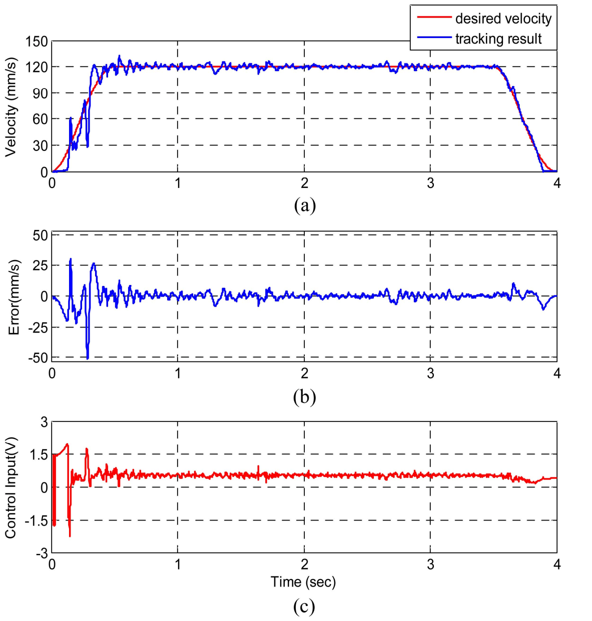

Fig. 14. Experimental results of AFNN-SMC+ H_∞ for trapezoidal velocity profile: (a) velocity control response; (b) control error; (c) control input.

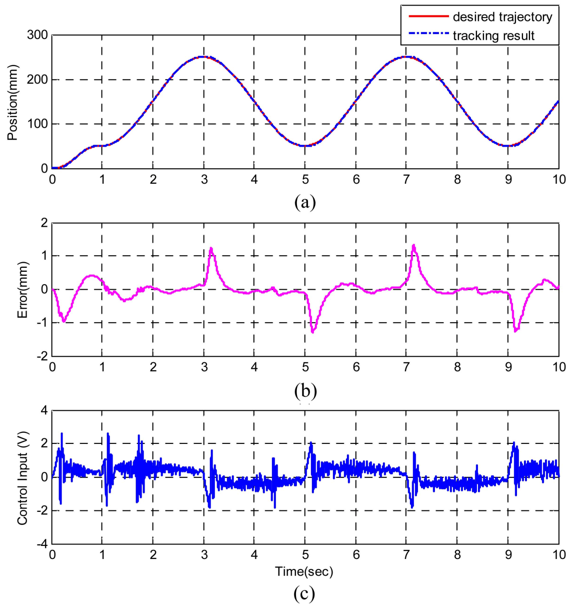

Fig. 15. Experimental results of AFNN-SMC+ H_∞ for sinusoidal trajectory with the payload changed from 6 kg to 13 kg: (a) position control response; (b) control error; (c) control input.

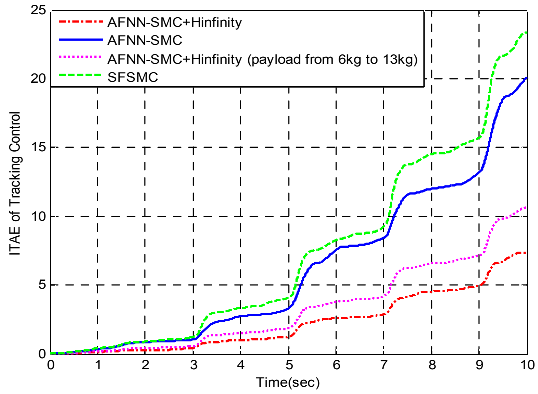

Fig. 16. Comparison of ITAE of tracking error for periodic sinusoidal tracking control of SFSMC, AFNN-SMC, AFNN-SMC+ H_∞ and AFNN-SMC+ H_∞ with payloads changed from 6 kg to 13 kg.

During the second phase the piston must maintain the desired velocity. During the third phase the piston must be decelerated so that all motion will stop prior to the piston reaching the end of the cylinder. Fig. 14 shows the experimental result of the AFNN-SMC+ H_∞ for the 120 mm/sec trapezoidal velocity profile. According to the experimental results, once the piston reaches the target velocity, the AFNN-SMC+ H_∞ appears to be able to provide adequate control performance. However, the controller does not perform well during the initial phase of the trapezoidal velocity profile. During the initial phase, when the pressure difference between the two chambers is large enough, the friction force will be overcome by the valve. Since the piston does not begin to move during this time, no enough error is produced between the desired and actual velocity. Therefore, the result is an initial lag in tracking the desired velocity.

5.5 Robustness tests

Robustness is very important for a practical control system. The concept of robustness is different from that of generality. Robustness is the ability of a control system to be insensitive to the variation of the plant parameters when using the nominal controller designed based on the nominal plant model, while generality means the control strategy design method can be applied to control systems with different dynamic. The nominal control strategies were designed for the Festo rodless PAS with a moving mass M = 6 kg. To test the robustness to the variation of the moving mass, we increased the moving mass to 13 kg without altering the nominal control strategies. The robustness of the proposed AFNN-SMC+ H_∞ was tested under different mass payload disturbances. Fig. 15 shows the trajectory tracking response, control effort and tracking error of the sinusoidal trajectory with payloads changed from 6 kg, as in Fig. 12, to 13 kg. With this change of the mass of the payload, only a slight increase in the tracking error occurs, and the tracking error can still keep within ± 1.5 mm. The test results verify that the robustness of the proposed the AFNN-SMC+ H_∞ is satisfied. In Fig. 16, the integral time absolute error ITAE $= \int t|e(t)|dt$ is used to measure the tracking error of the sinusoidal trajectory tracking for AFNN-SMC, SFSMC, AFNN-SMC+ H_∞, and AFNN-SMC+ H_∞ (payload is changed from 6 kg to 13 kg). Experimental results demonstrated that the AFNN-SMC+ H_∞ is very effective and ITAE is reduced by 63% on average.

6. Conclusions

We have developed the AFNN-SMC+ H_∞ and successfully applied it to the position regulation, trajectory tracking, and velocity control of the rodless PAS under different loading conditions. We chose AFNN as the identification technique because it has the elegant property of consisting of a family of orthogonal Fourier functions. That is, the structure of AFNN can be easily decided according to clear physical meaning. The proposed AFNN-SMC+ H_∞ has the following advantages: (1) It can reduce the serious chattering phenomenon and (2) based on the H_∞ tracking design technique, it can attenuate the uncertainties caused by the un-modeled dynamics, the approximation error and the external disturbance. Compared with AFNN-SMC, the AFNN-SMC+ H_∞ can result in a high tracking precision and reduce sensitivity to disturbance. The experimental results show our proposed AFNN-SMC+ H_∞ can overcome the AFNN-SMC in tracking and robust performances.

Acknowledgment

This work was supported by Ministry of Science and Technology, Taiwan, under Grant MOST 104-2221-E-262-015-, MOST 104-2918-I-234, and MOST 104-2221-E-234-001-. The authors would like to thank reviewers and the editor for their helpful and detailed comments that have assisted in improving the presentation of this paper.

References

[1] C. H. Lu, Y. R. Hwang and Y. T. Shen, Backstepping sliding-mode control for a pneumatic control system, *Proc. Inst. Mech. Eng., Part I J. Syst. and Control Eng.*, 224 (6) (2010) 763-770.

[2] J. E. Bobrow and F. Jabbari, Adaptive pneumatic force actuator and position control, *J. Dyn. Syst. Meas., Control*, 113 (1991) 267-272.

[3] B. W. McDonell and J. E. Bobrow, Adaptive tracking control of an air powered robot actuator, *J. Dyn. Syst. Meas., Control*, 115 (3) (1993) 427-433.

[4] R. Richardson, A. R. Plummer and M. D. Brown, Self-tuning control of a pneumatic actuator under the influence of gravity, *IEEE Trans. Control Syst. Technol.*, 9 (2) (2001) 330-334.

[5] J. Yao, Z. Jiao, D. Ma and L. Yan, High-accuracy tracking control of hydraulic rotary actuators with modeling uncertainties, *IEEE/ASME Trans. Mechatronics*, 19 (2) (2014) 633-641.

[6] J. Yao, Z. Jiao and D. Ma, A practical nonlinear adaptive control of hydraulic servomechanisms with periodic-like disturbances, *IEEE/ASME Trans. Mechatronics*, DOI: 10.1109/TMECH.2015. 2409893 (2015).

[7] J. Yao, Z. Jiao and B. Yao, Nonlinear adaptive robust backstepping force control of hydraulic load simulator: Theory and experiments, *Journal of Mechanical Science and Technology*, 28 (4) (2014) 1499-1507.

[8] S. Drakunov, G. D. Hanchin, W. C. Su and Ü. Özgüner, Nonlinear control of rodless pneumatic servo actuator, or sliding modes versus Coulomb friction, *Automatica*, 33 (3) (1997) 1401-1408.

[9] R. B. van Varseveld and G. M. Bone, Accurate position control of a pneumatic actuator using on/off solenoid valves, *IEEE Trans. Mechatronics*, 2 (3) (1997) 195-204.

[10] J. Wang, J. Pu, P. R. Moore and Z. Zhang, Modeling study and servo-control of air motor systems, *Int. J. Contr.*, 71 (3) (1998) 459-476.

[11] C. H Lu, Y. R. Hwang and Y. T. Shen, Backstepping sliding mode tracking control of a vane-type air motor X-Y table motion system, *ISA Trans.*, 50 (2) (2011) 278-286.

[12] J. Wang, Ü. Kotta and J. Ke, Tracking control of nonlinear pneumatic actuator systems using static state feedback linearization of the input–output map, *Proc. Estonian Acad. Sci. Phys. Math.*, 56 (1) (2007) 47-66.

[13] J. E. Slotin and W. Li, *Applied nonlinear control*, Prentice-Hall Inc, New Jersey (1991).

[14] H. I. Ali, S. B. Noor and B. M. M. H. Marhaban, A review of pneumatic actuators (Modeling and control), *Australian Journal of Basic and Applied Sciences*, 3 (2) (2009) 440-454.

[15] H. Lee, E. Kim, H.-J. Kang and M. Park, Design of a sliding mode controller with fuzzy sliding surfaces, *Proc. Inst. Elect. Eng.*, 145 (5) (1998) 411-418.

[16] Y. S. Lu and J. S. Chen, A self-organizing fuzzy sliding-mode controller design for a class of nonlinear servo systems, *IEEE Trans. Ind. Electron.*, 41 (5) (1994) 492-502.

[17] Q. P. Ha, D. C. Rye and H. F. Durrant-Whyte, Fuzzy moving sliding mode control with application to robotic manipulators, *Automatica,* 35 (1999) 607-616.

[18] S. B. Choi and J. S. Kim, A fuzzy-sliding mode controller for robust tracking of robotic manipulators, *Mechatronics,* 7 (2) (1997) 199-216.

[19] G. C. Hwang and S. C. Lin, A stability approach to fuzzy control design for nonlinear systems, *Fuzzy Sets Syst.,* 48 (3) (1992) 279-287.

[20] E. Richer and Y. Hurmuzlu, A high performance pneumatic force actuator system: Part I- Nonlinear mathematical model, *J. Dyn. Syst. Meas., Control*, 122 (2000) 416-425.

[21] E. Richer and Y. Hurmuzlu, A high performance pneumatic force actuator system: Part II- Nonlinear controller design, *J. Dyn. Syst. Meas., Control*, 122 (2000) 426-434.

[22] J. E. Bobrow and B. W. McDonell, Modeling, identification, and control of a pneumatically actuated, force controllable robot, *IEEE Trans. Robotics and Automation*, 14 (5) (1998) 732-742.

[23] F. C. Chen and C. C. Liu, Adaptively controlling nonlinear continuous-time systems using multilayer neural networks, *IEEE Trans. Autom. Control*, 39 (10) (1994) 1306-1310.

[24] F. C. Chen and H. K. Khalil, Adaptive control of a class of nonlinear discrete-time systems using neural networks, *IEEE Trans. Autom. Control*, 40 (5) (1995) 791-801.

[25] F. L. Lewis, A. Yesildirek and K. Liu, Multilayer neural-net robot controller with guaranteed tracking performance, *IEEE Trans. Neural Networks*, 7 (2) (1996) 388-398.

[26] S. Jagannathan and F. L. Lewis, Discrete-time neural net controller for a class of nonlinear dynamical systems, *IEEE Trans. Automatic Control*, 41 (10) (1996) 1693-1699.

[27] S. Jagannathan, Control of a class of nonlinear discrete-time system using multilayer neural networks, *IEEE Trans. Neural Networks*, 12 (5) (2008) 1113-1120.

[28] S. Jagannathan and P. He, Neural-network-based state-feedback control of a nonlinear discrete-time system in nonstrict feedback form, *IEEE Trans. Neural Networks*, 19 (12) (2008) 2073-2087.

[29] C. Yang, S. S. Ge, C. Xiang, T. Y. Chai and T. H. Lee, Output feedback NN control for two classes of discrete-time systems with unknown control directions in a unified approach, *IEEE Trans. Neural Networks*, 19 (11) (2008) 1873-1886.

[30] Y. C. Tsai and A. C. Huang, FAT-based adaptive control for pneumatic servo systems with mismatched uncertainties, *Mechanical Systems and Signal Processing*, 22 (2008) 1263-1273.

[31] T. Zhang, S. S. Ge and C. C. Hang, Adaptive neural network control for strict-feedback nonlinear systems using backstepping design, *Automatica*, 36 (12) (2000) 835-1846.

[32] W. Y. Wang, M. L. Chan, C. C. J. Hsu and T. T. Lee, H_∞ tracking-based sliding mode control for uncertain nonlinear systems via an adaptive fuzzy-neural approach, *IEEE Trans. Systems, Man, Cybernetics B*, 32 (4) (2002) 483-492.

[33] W. S. Chen and Z. Q. Zhang, Globally stable adaptive backstepping fuzzy control for output-feedback systems with unknown high-frequency gain sign, *Fuzzy Sets and Systems*, 161 (6) (2010) 821-836.

[34] C. F. Hsu, C. M. Lin and T. T. Lee, Wavelet adaptive backstepping control for a class of nonlinear systems, *IEEE Trans. Neural Networks*, 17 (5) (2006) 1175-1183.

[35] J. Li, W. S. Chen and J. M. Li, Adaptive NN output-feedback stabilization for a class of strict-feedback stochastic nonlinear systems, *ISA Trans*., 48 (4) (2009) 468-475.

[36] M. M. Polycarpou, Stable adaptive neural control scheme for nonlinear systems, *IEEE Trans. Automatic Control*, 41 (3) (1996) 447-451.

[37] W. Zuo and L. Cai, Adaptive-Fourier-neural-network-based control for a class of uncertain nonlinear systems, *IEEE Trans. Neural Networks*, 19 (10) (2008) 1689-1701.

[38] B. S. Chen, C. H. Lee and Y. C. Chang, H_∞ tracking design of uncertain nonlinear SISO systems: Adaptive fuzzy approach, *IEEE Trans. Fuzzy Systems*, 4 (1) (1996) 32-43.

[39] W. Zuo and L. Cai, Adaptive-Fourier-neural-network-based control for a class of uncertain nonlinear systems, *IEEE Trans. Neural Networks*, 19 (10) (2008) 1689-1701.

[40] W. Zuo, Y. Zhu and L. Cai, Fourier-neural-network-based learning control for a class of uncertain nonlinear systems with flexible components, *IEEE Trans. Neural Networks*, 20 (1) (2009) 139-151.

[41] Z. Yang, Z. Wei and L. Cai, Tracking control of a belt-driving system using improved Fourier series based learning controller, *Proc. of IEEE International Conference on Intelligent Robots and Systems* (2008) 881-886.

[42] B. W. Andersen, *The analysis and design of pneumatic systems*, Krieger Publishing Co., New York, USA (1976).

[43] J. F. Blackburn, G. Reethof and J. L. Shearer, *Fluid power control*, The Technology Press and Wiley, New York (1960).

[44] S. Armstrong-Helouvry, P. Dupont and C. Canudas De Wit, Friction in servo machines: Analysis and control methods, *Transactions of the ASME, J. of Application, Mechanics, and Reverend*, 47 (7) (1994) 275-306.

[45] S. Armstrong-Helouvry, P. Dupont and C. Canudas De Wit, A survey of models, analysis tools and compensation methods for the control of machines with friction, *Automatica*, 30 (1994) 1083-1183.

[46] W. Rudin, *Principles of mathematical analysis*, 3rd ed., McGraw-Hill Inc., New York, USA (1976).

[47] J. Huang and F. L. Lewis, Neural-network predictive control for nonlinear dynamic systems with time-delay, *IEEE Trans. Neural Networks*, 14 (2) (2003) 377-389.

[48] S. Lin and A. A. Goldenberg, Neural-network control of mobile manipulators, *IEEE Trans. Neural Networks*, 12 (5) (2001) 1121-113.

[49] J. Slotine and W. Li, *Applied nonlinear control*, Prentice Hall, Englewood Cliffs, N.J. (1991).

[50] W. Jihong, K. Ülle and K. Jia, Tracking control of nonlinear pneumatic actuator systems using static state feedback linearization of the input-output map, *Proceedings of the Estonian Academy of Sciences. Physics. Mathematics*, 56 (1) (2007) 47-66.

[51] W. Perruquetti, T. Floquet and P. Borne, A note on sliding observer and controller for generalized canonical forms, *Proc. of the 37th IEEE Conference on Decision and Control* (1998) 1920-1925.

[52] S. W. Kim and J. J. Lee, Design of a fuzzy controller with fuzzy sliding surface, *Fuzzy Sets and Systems*, 117 (3) (1995) 359-367.

Lian-Wang Lee received the M.S. in automation and control and the Ph.D. from National Taiwan University of Science and Technology, Taipei, in 2000 and 2009, respectively. He is an Assistant Professor with the Department of Mechanical Engineering, Lunghwa University of Science and Technology, Guishan, Taiwan. His research interests include fluid power control, nonlinear control, mechatronics, intelligent control, adaptive control, and sliding mode control.

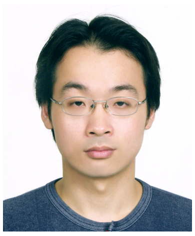

I-Hsum Li received the M.S. in electronic engineering form Fu-Jen Catholic University, Taipei, Taiwan, in 2001, and the Ph.D. at National Taiwan University of Science and Technology, Taipei, Taiwan, in 2007. He is an Associate Professor in the Department of Computer Science and Information Engineering in Lee-Ming Institute of Technology, Taiwan. His research interests include genetic algorithms, fuzzy logic systems, adaptive control, system identification and antilock braking system.